

Simulations of Superrotation on Slowly Rotating Planets: Sensitivity to Rotation and Initial Condition

ANTHONY D. DEL GENIO

NASA Goddard Institute for Space Studies, New York, New York 10025

E-mail: pdadd@giss.nasa.gov

AND

WEI ZHOU

Science Systems and Applications, Inc., Institute for Space Studies, New York, New York 10025

Received May 1, 1995; revised October 27, 1995

We use a simplified terrestrial general circulation model as a nonlinear process model to investigate factors that influence the extent of equatorial superrotation in statically stable atmospheres on slowly rotating planets such as Titan and Venus. The possibility of multiple equilibria is tested by running the same model to equilibrium from vastly different initial conditions. The final state is effectively independent of initial state, reinforcing the impression that equatorial superrotation is inevitable on slowly rotating planets with stable radiative equilibrium structures. Of particular interest is the fact that at Titan rotation, the model equilibrates with strong prograde winds even when initialized with strong retrograde winds. This suggests that reliable remote sensing inferences of latitudinal temperature gradients on Titan can unambiguously be interpreted as evidence for superrotation. We also demonstrate for the first time that significant equatorial superrotation can be produced at Venus' rotation rate in such models, given sufficient numerical precision. The strength of superrotating zonal winds increases with rotation rate in the slowly rotating regime when other parameters are held fixed. However, the efficiency of superrotation relative to the angular momentum of an atmosphere corotating with the solid planet increases with decreasing rotation rate instead, because the Hadley cell strengthens and expands poleward. This allows for the formation of stronger high latitude jets, which ultimately serve as the source for equatorial superrotation via barotropic instability. Estimates of relevant parameter settings for Triton and Pluto tentatively imply that their atmospheres may marginally be in the superrotating regime, but only if temperature decreases with height near the surface. © 1996 Academic Press, Inc.

1. INTRODUCTION

The phenomenon of equatorial superrotation observed or inferred in the atmospheres of the slowly rotating plan-

ets Venus and Titan presents one of the most formidable challenges to understanding in comparative planetary fluid dynamics. After a long history of failed attempts to produce superrotation in general circulation models (GCMs), success has been achieved recently, at least for the case of Titan's rotation rate (Del Genio *et al.* 1993, Hourdin *et al.* 1995). The more weakly rotating Venus case has been more difficult to simulate.

The key to superrotation in these simulations has been the presence of planetwide cloud cover at high altitude, a feature of both planets that had been previously neglected. The cloud absorbs significant amounts of sunlight, stabilizing the lapse rate and effectively detaching the cloud-level dynamics from the strong dissipation that occurs near the surface. Under these weakly dissipative conditions, upward and poleward transport of angular momentum by the Hadley circulation combined with equatorward eddy transport of momentum generated by barotropic instability of the high-latitude jet (Gierasch 1975, Rossow and Williams 1979) act efficiently to produce strong superrotation at all latitudes. The latitudinal profile of zonal wind resembles that implied by complete mixing of Ertel potential vorticity between the equator and the jet latitude (Allison *et al.* 1994).

A number of important questions still remain, however. In the superrotating regime, the zonal wind is nearly in cyclostrophic balance except perhaps near the surface. Since cyclostrophic balance is nonlinear in the zonal wind speed, in principle a given geopotential or temperature distribution can be balanced by zonal winds in either direction. For Venus, where unambiguous observations of superrotation exist, this is not an issue, but for Titan, where only indirect inferences have been reported to date (Flasar *et al.* 1981, Sicardy *et al.* 1990), the issue has not been put

to rest. In the GCMs, superrotation is clearly preferred, since the mechanism involves transfer of the planet's angular momentum into the atmosphere by the Hadley circulation. But this result is derived in the models from a resting initial state, and it is not obvious that a subrotating zonal wind distribution, produced by a different mechanism, might not be able to remain in thermal wind balance and represent an equally viable equilibrium configuration. This ambiguity has affected plans for tracking the descent of the upcoming Huygens probe of Titan (Flasar *et al.* 1995).

For Venus, the spinup of superrotation from rest raises somewhat different but related questions. Since other mechanisms (thermal tides, gravity waves) are also capable of producing some degree of superrotation, and such mechanisms are currently absent from GCMs, do previous failures to generate superrotation at Venus' rotation rate via the Gierasch mechanism depend at all on the absence of a background superrotating state? It might be true, for example, that a model initialized with observed Venus winds has stronger momentum sources and sinks and can thus maintain superrotation more easily than producing it. Related to this is the question of predictability of the nonlinear Venus dynamic state. Examples of multiple equilibria resulting from slightly different initial conditions in the coupled Earth atmosphere-ocean system have been produced (Marotzke and Willebrand 1991), and a transition to equatorial superrotation in simplified terrestrial models can be produced by modest changes in the forcing (Suarez and Duffy 1992).

Finally, even though it is now possible to simulate the superrotation phenomenon, the factors determining its magnitude are not yet understood. Gierasch's theory predicts a linear dependence of superrotation on rotation rate for a given depth of atmosphere and strength of vertical mixing. However, this applies only in the limit of extremely weak horizontal temperature gradients and maximally efficient horizontal mixing of vorticity, conditions which may not apply to the same degree or at all at different rotation rates in the slow rotation regime.

In this paper we test the sensitivity of superrotation in the GISS planetary GCM to both initial condition and rotation rate. The details of the model are given in Section 2. Sections 3 and 4 describe the results of simulations with different initial conditions and different rotation rates, respectively. The implications of our results for future modeling efforts, spacecraft missions, and other slowly rotating planets are discussed in Section 5.

2. MODEL DESCRIPTION

The version of the GISS GCM we use is similar in most respects to that described by Del Genio *et al.* (1993). Briefly, the GCM is a gridpoint model with $8^\circ \times 10^\circ$ hori-

zontal resolution and nine vertical layers with an upper boundary at 10 mbar pressure. Horizontal differencing uses the Arakawa B-grid but with potential temperature replacing temperature as a prognostic variable. The model uses no explicit vertical or horizontal diffusion. Radiative heating is computed with a semi-implicit spectral integration including all significant gases, aerosols, and cloud particles. Dry convective adjustment mixes heat between layers to remove superadiabatic lapse rates. Surface fluxes of heat and momentum are obtained from a drag-law formulation with a constant drag coefficient of 4×10^{-3} . Stratospheric drag at the upper boundary is excluded for all the experiments reported here but was included in some of the earlier simulations discussed in Del Genio *et al.* (1993).

The GCM is a terrestrial model (i.e., a 1-bar atmosphere with terrestrial atmospheric composition) rather than a direct simulation of Venus or Titan. To create a simplified nonlinear process model capable of exploring superrotation mechanisms, we remove the diurnal, seasonal, and hydrologic cycles, as well as topography and geographic variations. To create the stable radiative equilibrium structure necessary to promote superrotation, we prescribe an optically thick ($\tau = 5$ at $0.5 \mu\text{m}$ wavelength) planetwide cloud between the 150 and 550 mbar levels that mimics the solar absorption role of the planetwide cloud decks on both slowly rotating planets.

The simulations reported in this paper differ from those in Del Genio *et al.* (1993) in only two ways. First, for these runs we excluded momentum mixing by dry convection, an additional source of parameterized internal dissipation. The only explicit source of mechanical dissipation in the model is thus surface drag. This produces the most favorable possible setting for generating superrotation and simplifies the interpretation of energy cycle diagnostics, but tests with and without convective momentum mixing indicate that it actually has a negligible effect on the degree of superrotation achieved in the model. Second, the current simulations were performed on an IBM RISC6000 250T workstation, while those reported previously were run on an older Amdahl 5870 mainframe computer. Computations on the workstation are numerically more precise, and thus angular momentum is more closely conserved in the current runs and numerical dissipation reduced. This has virtually no effect on the simulation of the robust Titan superrotation regime, but it dramatically improves our ability to simulate superrotation in the weaker Venus rotation regime, as we will describe later.

For both Titan (16 days) and Venus (243 days) rotation periods, we ran the GCM to equilibrium twice, using identical physics but very different initial conditions to be described in the next section. For each run, equilibrium was judged by the temporal evolution of globally integrated angular momentum, which adjusts more slowly than other quantities such as eddy or zonal kinetic energy. Each simu-

lation was run for at least 10 years after achieving equilibrium; the results presented in this paper represent an average over the final 10 years. We also ran two additional experiments at rotation periods of 8 and 64 days to more fully sample the rotation dependence of superrotation within the quasi-barotropic Hadley regime.

3. SENSITIVITY TO INITIAL CONDITION

For the 16 day rotation period, we first ran a simulation starting from a resting, isothermal state; the equilibrium mean zonal wind field is shown in Fig. 1 (upper). Strong superrotation results at virtually all altitudes and latitudes, with equatorial wind speeds near cloud top (150 mb) $> 70 \text{ m sec}^{-1}$. This result is almost identical to that in earlier experiments (cf. Fig. 7a of Del Genio *et al.* 1993).

In this and every other slow rotation experiment con-

ducted with the current version of the GCM, the planetary rotation direction determines the eventual sign of the zonal wind, resulting in positive globally integrated angular momentum and net superrotation. This is not surprising, since Coriolis torques in the poleward branch of the Hadley cell are the source for the barotropically unstable high-latitude jets that drive the equatorial wind via equatorward eddy momentum fluxes. However, the equilibrium state is very close to gradient wind balance (typically within 5 m sec^{-1} ; cf. Fig. 14 of Del Genio *et al.* 1993). At slow rotation rates, the centrifugal term dominates the Coriolis term wherever the wind speed is strong, and so the balance is highly nonlinear. The gradient wind equation thus has a second solution characterized by retrograde, or subrotating, winds. In principle, the equilibrium geopotential field realized by the GCM might be able to maintain a balance with such a subrotating wind, at least above the planetary boundary layer, implying that observations of the temperature or geopotential height field on Titan would be ambiguous as to the sign of the balancing zonal wind.

To see whether such a solution is possible in the framework of the Gierasch mechanism, we calculated the retrograde gradient wind field corresponding to the final geopotential field from the experiment in Fig. 1 (upper). The resulting gradient wind is shown in Fig. 1 (lower). It is not the mirror image of the prograde solution, because the Coriolis force is not completely negligible at Titan's rotation rate and acts in the opposite direction of the centrifugal force. The net result of this competition is a very strong retrograde atmospheric rotation. This wind field was used to initialize an otherwise identical GCM simulation.

The transition of the global angular momentum to equilibrium is illustrated in Fig. 2 for both simulations. In Fig. 2, the angular momentum is normalized by that corresponding to solid body rotation, defining a dimensionless superrotation index S . Both experiments reach equilibrium in about 10 years, and the final state is almost identical in the two cases despite the vastly different initial conditions. The subrotating initial state case, in fact, equilibrates at slightly higher S than does the case initialized at rest, although the differences are small (4%). The final equilibrium wind field for the subrotating initial condition is shown in Fig. 3. It is strongly superrotating everywhere outside the boundary layer and closely resembles the result of the run started from rest.

This result makes sense in light of the Gierasch superrotation mechanism and the requirements for superrotation we previously found. Given the transfer of planetary angular momentum to the atmosphere via surface drag, the only way for a prograde rotating surface to equilibrate with a retrograde rotating atmosphere would be for the effect of the surface to be felt only within the boundary layer, but the Gierasch mechanism starts with upward redistribution of angular momentum by the Hadley cell.

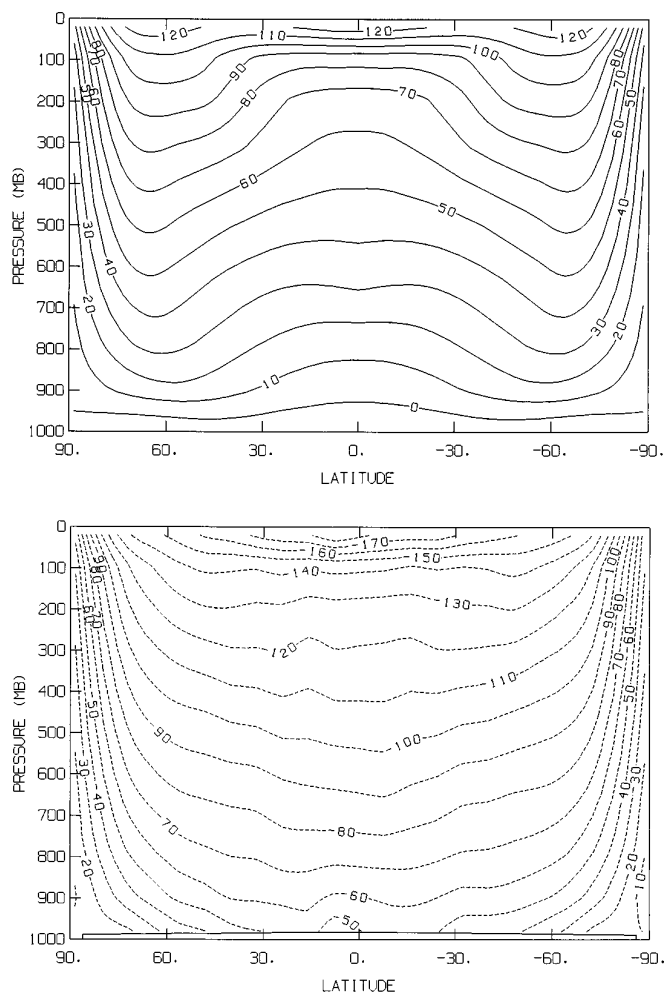


FIG. 1. (Upper) Equilibrium time and zonal mean zonal wind field for the simulation at the 16 day rotation period starting from rest. (Lower) Retrograde gradient wind balancing the final geopotential field for the 16 day simulation.

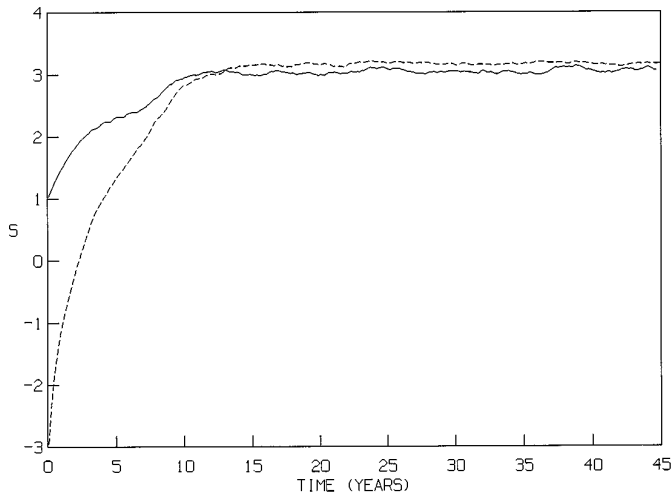


FIG. 2. Time evolution of superrotation index S (globally integrated angular momentum normalized by that for solid body rotation) for simulations at the 16 day period starting from rest (solid line) and from the subrotating initial state in Fig. 1, lower (dashed line).

Since a stable thermal structure is also necessary for superrotation, and this occurs on Titan because of an absorbing high-level cloud, forcing for the Hadley cell exists throughout the depth of the troposphere. The effect of the surface is thus inevitably communicated to the free troposphere, and initial subrotation is converted to superrotation in less than 5 years. It is worth noting that due to local maxima in radiative heating both within the cloud layer and near the surface, the GCM produces not a single Hadley cell but a series of three vertically stacked cells, with cloud-level and surface Hadley cells separated by a mid-troposphere thermally indirect circulation (cf. Figs. 3, 4, and 13 of Del

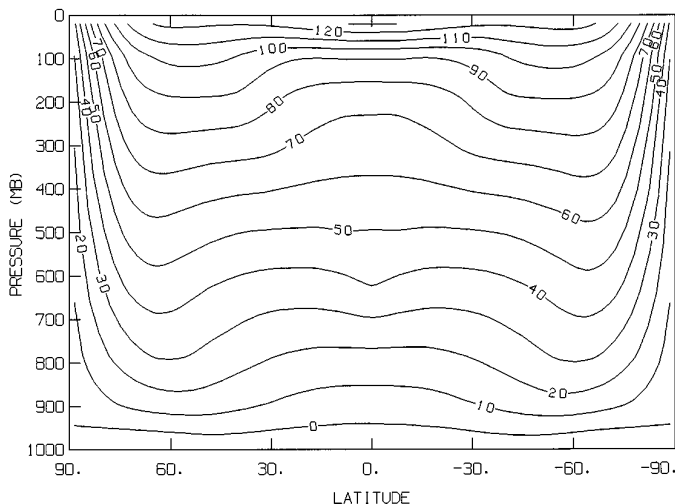


FIG. 3. As in Fig. 1 (upper) but for the run initialized with the retrograde gradient wind.

Genio *et al.* 1993). The reverse cell is sufficiently weak, though (in the absence of strong indirect forcing), that it does not qualitatively impede the transport of equatorial angular momentum to the upper troposphere by the mean circulation (cf. Fig. 8c of Del Genio *et al.*, 1993).

The role of the surface drag as a source of angular momentum is crucial here. Flasar and Conrath (1992), using kinematic arguments, show that angular momentum conserving flow toward low pressure, if initialized with a retrograde tangential velocity whose magnitude U exceeds the planetary rotational velocity Ωa (where Ω is the planetary angular velocity and a the planetary radius), will remain retrograde. In our simulation with initial subrotation, $U > \Omega a = 29 \text{ m sec}^{-1}$ over most of the atmosphere. Our experiment is thus a fairly stringent test of the ability of a subrotating flow to maintain itself in the presence of surface-atmosphere angular momentum exchange.

It might be argued that a better test would involve reversing the latitudinal temperature and geopotential gradients, so that the initial radiative heating would not immediately generate a Hadley cell. However, cyclostrophic balance cannot exist around a high, and so a retrograde gradient wind balance could not have a wind strong enough for the centrifugal force to exceed the Coriolis force. The upper limit for the magnitude of such a wind is $U = 2\Omega a$, which is 58 m sec^{-1} for the GCM (whose radius equals Earth's) and only 23 m sec^{-1} for Titan, both considerably slower than the retrograde wind that can be in balance around a low.

A somewhat different pair of experiments was performed at Venus' rotation rate. First, the GCM was started from a resting isothermal initial state; the equilibrium zonal wind field is shown in Fig. 4 (upper). As in the Titan rotation case, superrotation occurs at virtually all latitudes and altitudes, but at a lower wind speed. Cloud top equatorial wind speeds reach 10 m sec^{-1} , an order of magnitude stronger than previous GCM simulations of the Venus rotation regime with or without a stabilizing upper cloud layer. Next, we initialized a second simulation at Venus rotation with the final, strongly superrotating zonal wind field from the first Titan simulation (the time mean of which is shown in Fig. 1, upper). The resulting equilibrium wind field, shown in Fig. 4 (lower), is virtually indistinguishable from that for the run started from rest. The time evolution of the global angular momentum for the two simulations is shown in Fig. 5. The time mean angular momentum for the two cases differs by only 3.5%, comparable to random interannual fluctuations. For all intents and purposes, then, superrotation appears to be a robust feature of the atmospheres of stable, slowly rotating planets, independent of initial state.

Our Venus cases exhibit much stronger equatorial superrotation than we had previously been able to achieve (cf. Fig. 7c of Del Genio *et al.* 1993). Sensitivity tests indicate

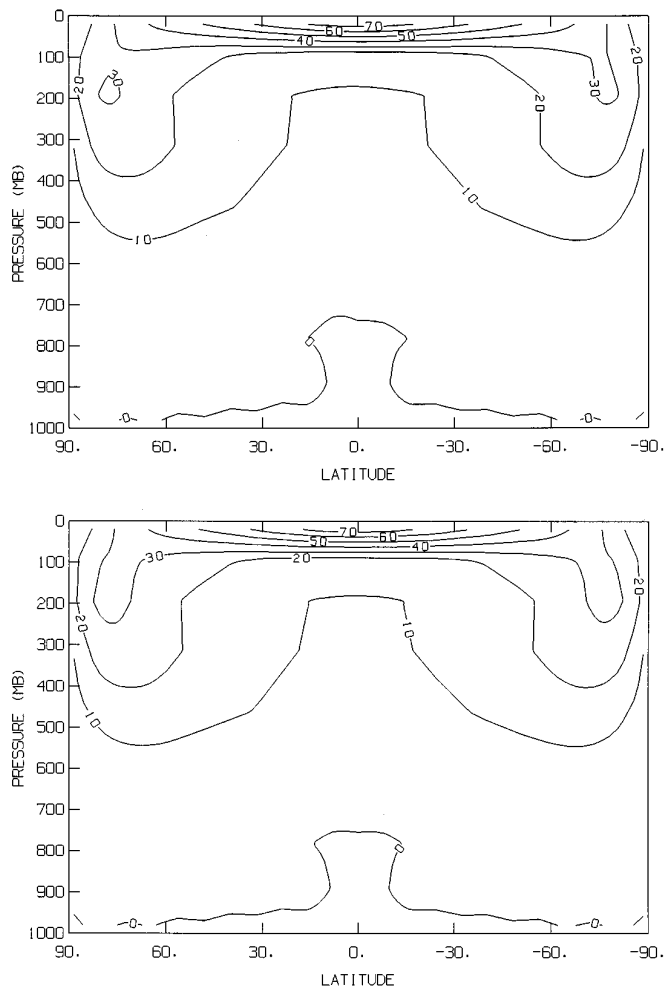


FIG. 4. As in Fig. 1 (upper) but for simulations at the 243 day period started from rest (upper) and from a superrotating initial state (lower).

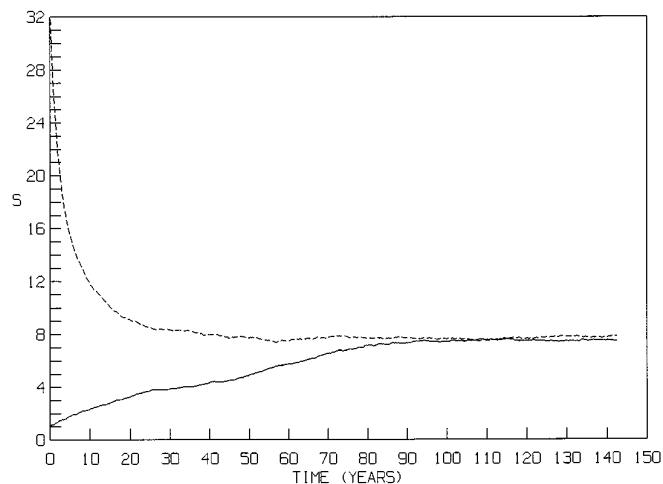


FIG. 5. As in Fig. 2 but for runs at the 243 day period started from rest (solid line) and from a superrotating initial state (dashed line).

that the absence of momentum mixing by convection has almost no global effect. The only other difference between the current and previous simulations is the machine used to perform the computations. The simulations in Del Genio *et al.* (1993) were done on a mainframe computer whose computations were single precision with the last digit truncated. The current computations were done on a workstation with inherently double precision calculations and with the final digit rounded off instead. These differences do not matter at terrestrial or Titan rotation rates, but they are apparently crucial at Venus' rotation rate, where individual terms in the momentum balance are two orders of magnitude smaller than at terrestrial rotation. The angular momentum sink by numerics is about 3%/year on the mainframe, but only 2%/year on the workstation. The time mean angular momentum reached in the mainframe experiment is less than 50% that in the workstation experiment. Furthermore, when run from a superrotating initial state, the mainframe version equilibrates to a different final state, with about 80% the angular momentum of the workstation versions. Clearly more attention needs to be paid to the angular momentum conserving features of numerical techniques used in dynamical models of the slowly rotating regime (cf. Hourdin and Talagrand 1995), but the consistency of our current results regardless of the initial condition suggests that the model is sufficiently accurate to reproduce most aspects of superrotation. One exception is the surface wind distribution, which produces nonzero net surface torque if angular momentum is not perfectly conserved by all components of the dynamics.

4. SENSITIVITY TO ROTATION RATE

Figure 6 displays the mean zonal wind field for experiments starting from rest but at rotation periods of 8 and 64 days. Comparing to Figs. 1 (upper) and 4 (upper), we see that superrotation at a 64 day period is intermediate in strength to that at 16 and 243 day periods, as expected. Superrotation at an 8 day period, on the other hand, is only slightly stronger than at a 16 day period. In the theory of Gierasch (1975), equatorial zonal wind speed scales linearly with rotation rate for fixed depth of atmosphere and strength of vertical mixing. Thus, equatorial winds should be a factor of 15 weaker at Venus' rotation rate than at Titan's, since the experiments differ only in their rotation rates. The realized equatorial zonal winds in the simulations, though, differ by only a factor of 6.

To quantify these differences we use the superrotation factor S , defined earlier as the ratio of globally integrated atmospheric angular momentum to that corresponding to solid body corotation. Per unit mass, the latter quantity is equal to $2\Omega a^2/3$. Thus, $S > 1$ indicates an atmosphere with net angular momentum relative to one at rest. Another convenient reference point is $S = 2$, which is characteristic

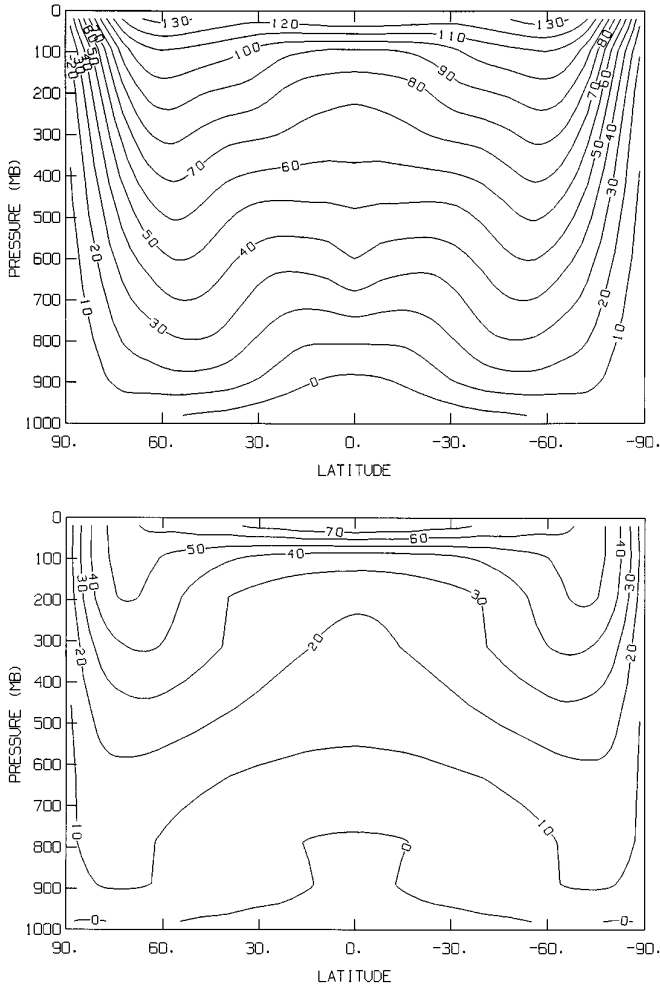


FIG. 6. As in Fig. 1 (upper) but for simulations started from rest at the 8 day (upper) and 64 day (lower) period.

of an atmosphere with a latitudinal wind profile determined by angular momentum conservation of a parcel displaced from equator to pole (Hourdin and Talagrand 1995). $S = 2$ is the maximum value that can be produced by an axially symmetric circulation; $S > 2$ is thus evidence of eddy effects on the mean zonal wind field. The upper curve in Fig. 7 shows S as a function of rotation period $P = 2\pi/\Omega$ for the four simulations at different rotation rates. Although the absolute magnitude of superrotation increases with increasing Ω , the efficiency of superrotation (as measured by S) increases with increasing P . At an 8 day period, there is almost no net effect of the eddies, while at longer periods, the eddies have a substantial global impact on angular momentum.

The GCM simulations differ from Gierasch's theory in that horizontal mixing in the GCM does not produce uniform angular velocity, but this does not appear to explain the simulated rotation rate dependence. The depth of the

atmosphere is virtually constant among the four experiments. The strength of vertical mixing is not, although the implied effective "vertical viscosity" associated with eddy motions (defined as the ratio of the vertical eddy flux to the vertical gradient of angular momentum) is similar in the experiments. The answer appears instead to depend on the horizontal heat and momentum balances. To understand the operative dynamics, consider first the atmospheric energy cycle for each simulation (Fig. 8). In all four, the energy cycle proceeds clockwise, with generation (G) of available potential energy (A) by differential insolation, conversion (C_A) of A to zonal kinetic energy (K_Z) by the Hadley cell, conversion (C_Z) of zonal to eddy kinetic energy (K_E) by barotropic instability, and associated conversion of K_E to A , i.e., negative baroclinic conversion (C_E). In each case, barotropic conversion greatly exceeds

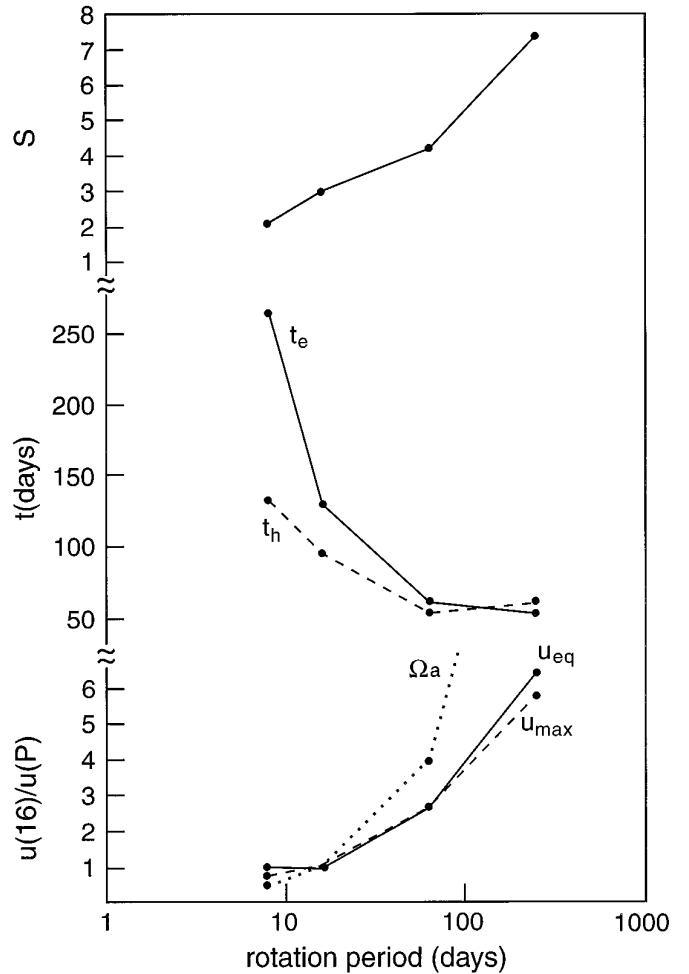


FIG. 7. Superrotation diagnostics vs rotation period for the simulations from rest at $P = 8, 16, 64$, and 243 days. (Upper) Superrotation index S . (Middle) Eddy (t_e , solid line) and Hadley (t_h , dashed line) time scales. (Lower) Zonal wind indices at 16 days divided by their values at each P : u_{eq} (solid line), u_{max} (dashed line), Ωa (dotted line).

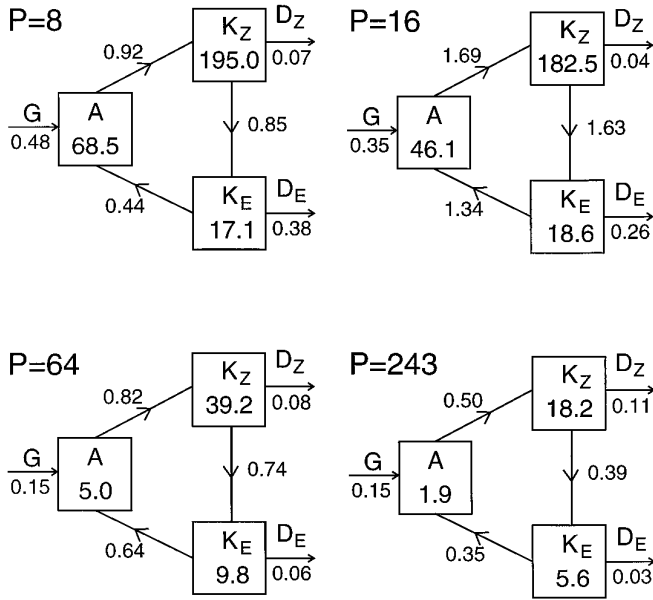


FIG. 8. Energy cycle diagnostics (as defined by Lorenz 1967) for the four simulations from rest. Energy reservoirs (boxes) in 10^5 J m^{-2} , conversion rates (arrows) in W m^{-2} .

dissipation (D_Z), which we had previously found to be necessary for strong equatorial superrotation. The energy cycle is most vigorous at $P = 16$ days, as judged by the magnitude of conversion rates, even though the energy reservoirs are greatest at $P = 8$ days. The explanation for this behavior differs for rotation periods less than and greater than 16 days.

At faster rotation rates, the GCM begins the transition from the quasi-barotropic to the baroclinic regime. Figure 9 compares the spectrum of baroclinic and barotropic conversion for 8 and 16 day periods. At 16 days, barotropic conversion is positive and baroclinic conversion negative at all zonal wavenumbers n . But at 8 days, barotropic conversion is negative and baroclinic conversion positive at $n = 1$, because the Rossby radius of deformation is comparable to the size of the planet at this period. Thus, baroclinic instability is possible for planetary-scale disturbances, and the associated poleward momentum transport partly offsets the effect of equatorward momentum transport at higher wavenumbers. At 8 days, there is in fact a distinct region of net poleward eddy momentum transport (not shown) poleward of 60° latitude, a feature not seen in the other three experiments.

At slower rotation rates, different physics operates. As noted before, the magnitude of the equatorial zonal wind should decrease with increasing rotation period, all other things being equal, but the efficiency of superrotation S increases. To see why, we examine the streamfunction of the mean meridional circulation for each of the experiments (Fig. 10). At the 8 day period, the Hadley cell ex-

tends only up to about 60° latitude, and is quite weak poleward of 30° ; in the polar regions a weak but noticeable Ferrel cell exists, consistent with the poleward eddy momentum flux at these latitudes. As rotation rate decreases in Fig. 10, the Hadley cell generally strengthens and expands to higher latitudes. A better indicator of the effective width of the Hadley cell is the position of the high latitude jet maximum. As can be seen from Figs. 1 (upper), 4 (upper), and 6, the jet position in the upper troposphere moves from 55° latitude at $P = 8$ days to 63° , 70° , and 78° latitude (an increment of one GCM gridbox in each case) for $P = 16$, 64, and 243 days, respectively.

The strengthening and poleward expansion of the Hadley cell as rotation rate decreases have opposite effects on superrotation efficiency. Gierasch (1975) highlighted the relative strength of equatorward eddy angular momentum transport and poleward Hadley cell angular momentum transport as an important factor for superrotation. In Gierasch's theory, the eddy term dominates, while in the GCM simulations, eddy and Hadley cell transports are similar in magnitude instead, but the relative strength of eddy and

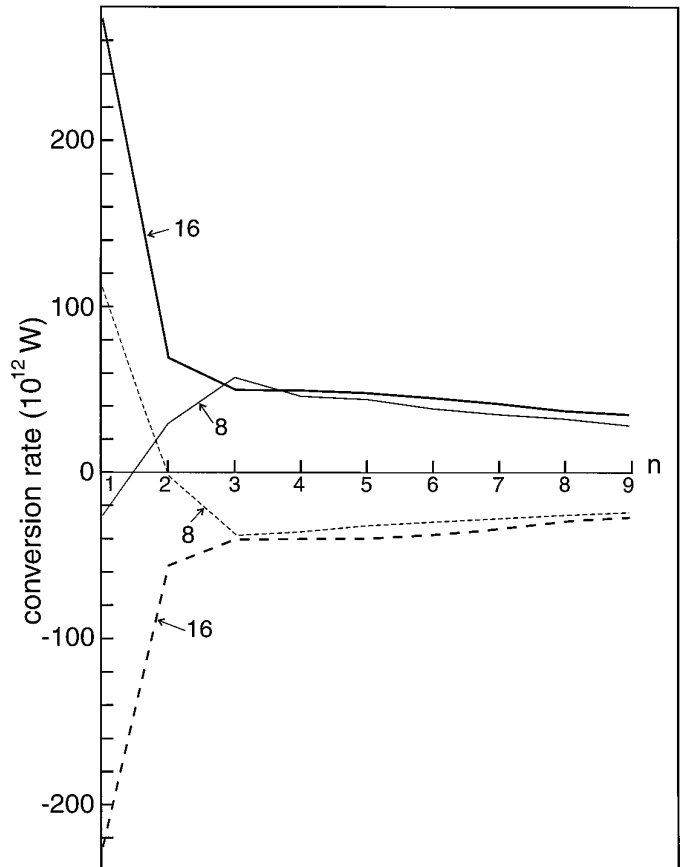


FIG. 9. Zonal wavenumber spectrum of barotropic conversion (solid lines) and baroclinic conversion (dashed lines) rates for the simulations from rest at $P = 8$ days (light lines) and 16 days (bold lines).

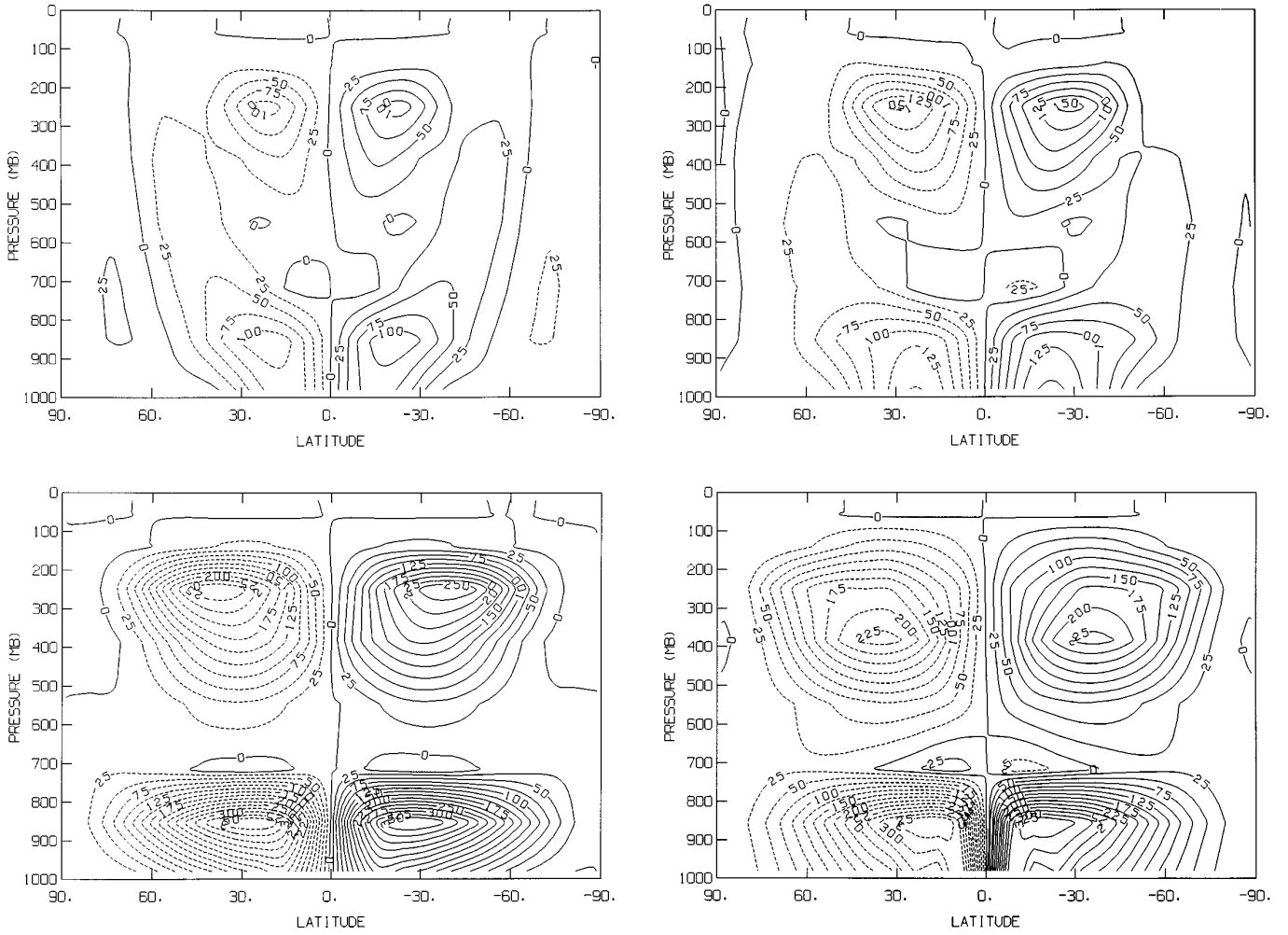


FIG. 10. Mass streamfunction of the mean meridional circulation for the four simulations started from rest. (Upper left) $P = 8$ days; (upper right) $P = 16$ days; (lower left) $P = 64$ days; (lower right) $P = 243$ days.

Hadley cell contributions does systematically change with rotation rate. We define a time scale for barotropic eddy conversion of K_Z to K_E by

$$t_e = K_Z / C_Z, \quad (1)$$

and a Hadley cell overturning time for the cloud level cell as

$$t_h = A \Delta p / \psi g, \quad (2)$$

where A is the area of the hemisphere, $\Delta p = 500$ mb the depth of the cloud level cell, g the acceleration of gravity, $A \Delta p / g$ the mass of atmosphere within the Hadley cell in each hemisphere, and ψ the peak mass streamfunction of the Hadley cell (in kg sec^{-1}).

Figure 7 (middle) displays the eddy and Hadley time scales as a function of rotation period. Both time scales

generally decrease with increasing rotation period. The decrease of t_h reflects the strengthening of the Hadley cell and by itself works against efficient superrotation, according to Gierasch's theory, but the rate of decrease of t_e is much faster. At the slowest rotation rates, $t_e \leq t_h$, and thus the efficiency of superrotation increases.

The decrease of t_e with decreasing rotation rate may depend on the latitudinal width of the Hadley cell instead. First note that as P increases, t_h becomes comparable to P at 64 days and much shorter at 243 days; this is consistent with the Hadley cell stretching almost to the pole at the longest rotation period. Within the upper branch of a Hadley cell, angular momentum is approximately conserved by poleward motion. Thus, a parcel drifting poleward starting from the equator at rest would generate a latitudinal profile of zonal wind u_m given by

$$u_m = \Omega a \sin^2 \theta / \cos \theta, \quad (3)$$

where θ is the latitude. The maximum value of this wind thus depends on the poleward extent of the Hadley cell (θ_{\max}) as well as rotation rate. Since θ_{\max} increases as Ω decreases, the effect of rotation rate on $u_{\max} = u_m(\theta_{\max})$ is lessened. In other words, poleward drift in the Hadley cell can generate higher instantaneous jet speeds as rotation decreases than is predicted simply by the linear dependence on Ω . Thus, more zonal kinetic energy is produced and more vigorous barotropic conversion results.

That this is relevant to the degree of equatorial superrotation achieved in the simulations is suggested by the lower curves in Fig. 7. Plotted here are ratios of zonal wind speed at the 16 day period to that at other rotation periods for three different quantities: the actual cloud top equatorial wind speed realized by the GCM (u_{eq}), the theoretical value u_{\max} for the maximum jet speed, and the zonal wind speed of equatorial planetary rotation Ωa . The rotation dependence of u_{eq} tracks that of u_{\max} remarkably well, while the rotation rate alone is a less accurate predictor of superrotation strength. Hadley cell extent may therefore be ultimately responsible for the increasing efficiency of superrotation with decreasing rotation rate.

K_E contains contributions from eddies of all spatial scales, only some of which are associated with the barotropic instability that is responsible for the superrotation. The spatial structure of the important eddies can be portrayed by calculating a “correlated eddy amplitude” $\sqrt{u'v'}$, which isolates the magnitudes of only those eddies that accomplish the equatorward angular momentum transport (Fig. 11). Peak eddy amplitudes at both $P = 16$ and 243 days are $\sim 10\text{--}15\text{ m sec}^{-1}$ and occur near cloud top in mid-latitudes in these experiments. The peak occurs near 30° latitude at the 16 day period but near 60° latitude at 243 days; the 16 day simulation has a second clear peak at low altitudes that is not evident at 243 days.

Our results cannot be compared directly with observations, since they are the product of an idealized slowly rotating terrestrial model rather than an actual Venus or Titan simulation. However, it is worth noting that Pioneer Venus OCPP cloud-tracked winds in Spring 1985, a period of increasing equatorial zonal wind speed, exhibit equatorward eddy momentum fluxes with peak eddy amplitudes of 11 and 7 m sec^{-1} at 40°S and 20°N , respectively (cf. Table 9 of Rossow *et al.* 1990). The GCM thus bears a resemblance to some of the available observations. (Note that cloud-tracked wind data do not exist as far poleward as 60° , where the highest eddy amplitudes in the GCM occur.)

In other epochs, though, weak poleward eddy fluxes are observed by OCPP at cloud top instead. Our simulations suggest two possible explanations for this. First, the altitude of peak eddy amplitude is sensitive to dissipation. In the experiments reported here, stratospheric drag is absent, so eddy amplitude peaks at cloud top. In earlier experiments that included stratospheric drag, the eddies peaked

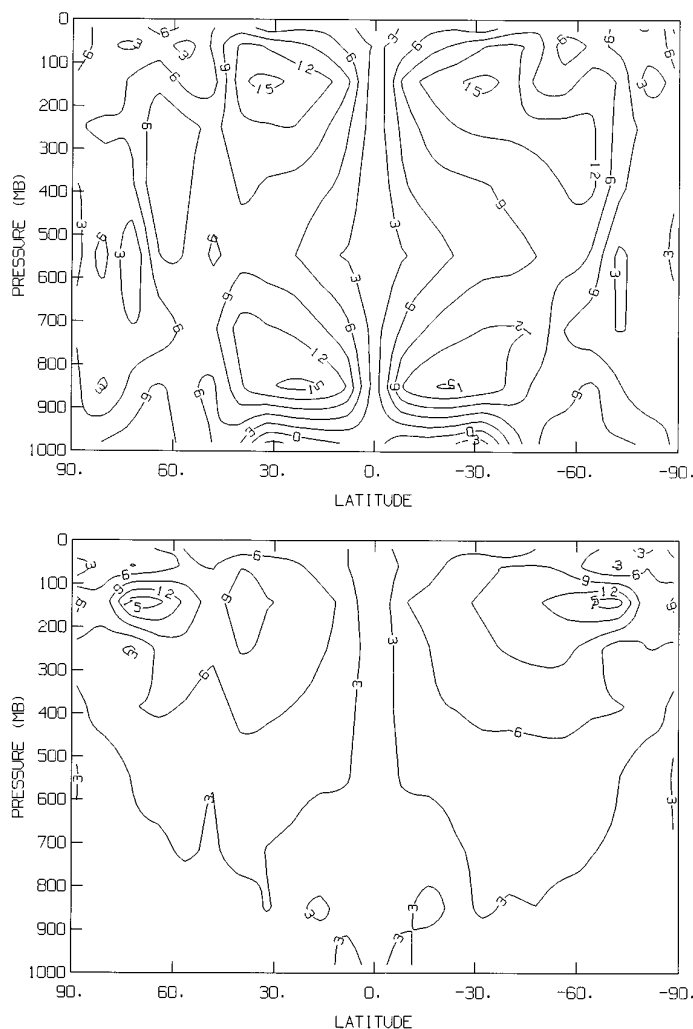


FIG. 11. Mean amplitude of eddies contributing to the equatorward eddy angular momentum flux for the simulations at $P = 16$ days (upper) and 243 days (lower).

at deeper levels, near cloud base (cf. Fig. 8b of Del Genio *et al.* 1993). On Venus, thermal tides act to decelerate the flow above cloud top, so the contribution of barotropic instability may occur primarily below the visible cloud level. Furthermore, in a turbulent flow at slow rotation, the net eddy flux is a small residual between large instantaneous correlations of opposite sign at different longitudes. Although the GCM produces a clear signal of equatorward eddy momentum flux in the zonal and time mean, the associated tilt of the streamlines is not obvious in a snapshot of the flow field (Fig. 12). At the instant depicted in Fig. 12, the zonal mean eddy flux is equatorward at all latitudes but one between $12^\circ\text{--}43^\circ$ in both hemispheres, yet only 198 out of 360 gridboxes (55%) contribute an equatorward flux. Thus, cloud-tracked winds, which are inevitably a sparse sample of the flow field, may not always

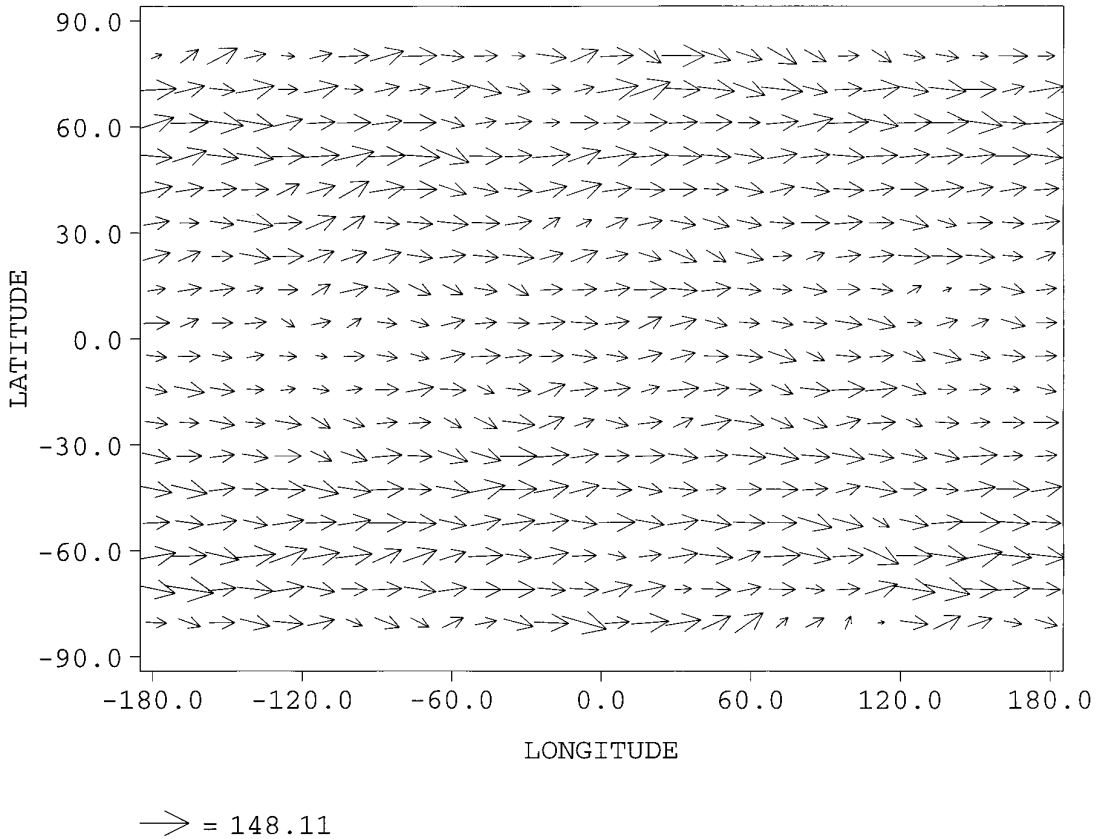


FIG. 12. Map of a representative instantaneous flow field simulated by the GCM near cloud top (200 mb) at $P = 16$ days. The size of the vectors indicates the wind speed (based on the scale at the lower left, in m sec^{-1}) and the orientation of the instantaneous wind direction.

reliably indicate the true direction of the eddy momentum flux unless a sufficiently large number of vectors are measured.

5. DISCUSSION

Because temperature and oblateness observations are ambiguous as to the sign of the zonal wind on Titan, the Cassini/Huygens project has adopted a very conservative envelope for possible drift of the Huygens entry probe that allows for both strongly superrotating and subrotating possibilities (cf. Flasar *et al.* 1995). This roughly doubles the uncertainty in the location of the probe landing site relative to a superrotation-only assumption, with implications for antenna design and data rate for the mission. The results presented here suggest that Cassini/Huygens science return could be greatly increased with little additional risk by assuming only prograde probe drift scenarios. The weak latitudinal temperature gradients observed by Voyager, combined with solar heating caused by the planetwide stratospheric cloud, are strong evidence for a Hadley cell. In the presence of such a cell and its attendant upward momentum transport, it seems inevitable that the

effect of the prograde rotation of the solid planet will determine the sense of atmospheric rotation on Titan.

This is not to say that the possibility of multiple equilibria can be ruled out by our experiments. The terrestrial ocean-atmosphere system, which can exhibit multiple equilibria, is probably not relevant here, because its intransitivity is associated with competing temperature and salinity effects on buoyancy, a situation with no analog on the slowly rotating planets. Of greater potential interest is the simple terrestrial atmosphere model of Suarez and Duffy (1992), which exhibits multiple equilibria in the presence of sufficiently strong hemispherically asymmetric forcing. Such forcing is unlikely for Venus, but more plausible for Titan, which has large seasonality. What is needed is a mechanism by which such forcing could produce poleward eddy momentum transport at low latitudes, countering the effect of the quasi-barotropic eddies we have simulated. With such forcing, weak equatorial winds might be possible. Extensive methane cumulus convection, which would increase vertical mixing, might also suppress the tendency for equatorial superrotation.

Our results also have practical implications for the understanding of superrotation on Venus. Previous studies

have shown that thermal tides can generate significant superrotation in Venus' upper atmosphere, but not in the lower atmosphere; such models must assume a background superrotation at the lower boundary (Newman and Leovy 1992). The Gierasch mechanism is a logical candidate to produce such background superrotation, but in practice it had not before been successful in doing so in GCMs run at the extremely slow Venus rotation rate. Our results, though restricted to a shallow atmosphere, are much more encouraging. The GCM now produces an atmosphere with more than 7 times the angular momentum of one at rest, compared to the observed value $S = 10$, while the simulated vertical shear is about half that observed (cf. Schubert *et al.* 1980). Consequently, the substantial computational investment required for an actual Venus GCM (because of the large number of layers required and the long radiative time constant) may now be justified.

Our findings on superrotation magnitude vs efficiency also have implications for comparative planetology. If superrotation efficiency increases with decreasing rotation rate because the Hadley cell expands toward the pole, then efficiency cannot increase indefinitely. In our experiments at the 243 day period, the jet is already within 10° – 15° of the pole. Thus, Venus may be close to the theoretical maximum superrotation efficiency possible on a slowly rotating planet. Furthermore, as superrotation increases, the “effective” rotation rate felt by the mean meridional circulation through poleward advection of total (planetary + relative) angular momentum increases, and this may act to confine the Hadley cell and the jet to lower latitudes. Venus observations, for example, suggest that the jet above the cloud tops is centered at 55° latitude instead (Newman *et al.* 1984). This interaction between zonal wind strength and jet location may be the self-limiting feature that ultimately determines the peak equatorial zonal wind speed. This is not inconsistent with the view that superrotation is limited by the strength of vertical mixing, because the agents of vertical mixing are likely to be large-scale eddies associated with those producing the superrotation at cloud level.

At the other end of the slowly rotating regime, our results suggest that at rotation rates much greater than Titan's, baroclinic instability at planetary scales begins to offset the effects of equatorward fluxes by barotropically unstable eddies at higher wavenumbers. The exact transition point depends on planetary radius and thermal structure, occurring at a period for which the Rossby radius of deformation approximately matches the planetary radius (Del Genio *et al.* 1993). If so, then Titan may be close to the upper limit for absolute magnitude of superrotation for an atmosphere of a given depth.

The transition between the baroclinic and quasi-barotropic regimes, somewhere between Earth's and Titan's rotation rates, is of considerable interest in this regard.

The only known planets with atmospheres within this range are Triton and Pluto, each of which rotates with a period near 6 days. The vertical thermal structure of the atmospheres of these planets is quite uncertain, but the standard model for both planets consists of an isothermal layer underlain by a sharp thermal inversion in the first few kilometers above the surface (cf. Tyler *et al.* 1989, Lellouch 1994). This combination works both for and against superrotation and cyclostrophic dynamics. The high static stability implied by such a profile promotes superrotation, but a very stable lapse rate near the ground reduces the surface drag coefficient and thus inhibits the atmosphere's source of angular momentum. Yelle *et al.* (1991) propose instead that low-altitude turbulence creates a layer of decreasing temperature with height on Triton up to a “tropopause” altitude of 8 km that matches the penetration depth of the plume observed at -50° latitude in Voyager images. In the Yelle *et al.* model, the lapse rate below 8 km is close to the moist adiabat for N_2 , but condensation takes place only within the plume, consistent with Voyager imagery. Thus, large-scale atmospheric motions “see” a statically stable structure, yet surface drag is greater than in the near-surface inversion scenario, the optimum setting for superrotation.

Using Triton as an example, we can estimate the Rossby radius of deformation $L_d = NH/f$, where $N = (g\Theta^{-1}d\Theta/dz)^{1/2}$ is the Brunt-Väisälä frequency, Θ is potential temperature, z is altitude, H is the scale height, and $f = 2\Omega \sin \theta$. Assuming that the static stability is the difference between the dry and moist adiabatic lapse rate, $d\Theta/dz = 0.76 - 0.12 = 0.64 \text{ K km}^{-1}$, and taking $g = 0.79 \text{ m sec}^{-2}$, $\Theta = 38 \text{ K}$, $H = 14.8 \text{ km}$, and $f = 1.9 \times 10^{-5} \text{ sec}^{-1}$ at -50° latitude (Ingersoll and Tryka 1990), we get $L_d = 2841 \text{ km}$, more than twice Triton's radius $a = 1352 \text{ km}$. Thus it seems likely that Triton's dynamics is in the quasi-barotropic Hadley regime; a similar suggestion for Pluto was first made by Stern and Trafton (1984). Taking $du/dz = 20 \text{ m sec}^{-1}/8 \text{ km}$ (Ingersoll 1990), we estimate a Triton Richardson number $Ri = N^2/(du/dz)^2 \approx 2$. Potential vorticity mixing constraints (Allison *et al.* 1994) then imply an equatorial zonal wind $u_{eq} \approx u(50^\circ) - \Omega a(1 - \cos 50^\circ) \approx 10 \text{ m sec}^{-1}$, placing Triton in the superrotating regime. On the other hand, if there is a near-surface inversion layer, $Ri \gg 2$, and the potential vorticity arguments then dictate an angular momentum-conserving latitudinal profile of wind. In this case, a 15 m sec^{-1} wind at -50° implies $u_{eq} \approx 0$, i.e., no equatorial superrotation, as can be seen by applying Eq. (3).

Note, though, that the Rossby number at -50° is $Ro = U/fL \approx 0.5$ (where the length scale L is the wavelength/ π for a wavenumber 1 disturbance), intermediate between the limits for geostrophic and cyclostrophic scaling. Thus, the dynamics may exhibit characteristics of the slowly rotating regime equatorward of the plume latitude but char-

acteristics of the baroclinic regime at high latitudes, as in our $P = 8$ days experiment. Similar considerations in principle apply to Pluto. The extreme seasonality of both planets complicates the picture, though, much as it does for Titan (Hourdin *et al.* 1995).

Unfortunately, no low-latitude observations of atmospheric motions above the boundary layer exist for Triton, and there has been no direct visual confirmation of superrotation on Titan either. The Titan issue should be settled definitively by several instruments on the Cassini/Huygens mission, if not sooner by Hubble Space Telescope imaging. However, it now seems plausible that Venus, which has historically been viewed as an anomaly by the atmospheric dynamics community, may instead represent the most common dynamical regime among the planets of our Solar System.

ACKNOWLEDGMENTS

We thank Mike Allison for helpful discussions and two anonymous reviewers for constructive suggestions. This work was supported by the NASA Planetary Atmospheres Program.

REFERENCES

- ALLISON, M., A. D. DEL GENIO, AND W. ZHOU 1994. Zero potential vorticity envelopes for the zonal-mean velocity of the Venus/Titan atmospheres. *J. Atmos. Sci.* **51**, 694–702.
- DEL GENIO, A. D., W. ZHOU, AND T. P. EICHLER 1993. Equatorial superrotation in a slowly rotating GCM: Implications for Titan and Venus. *Icarus* **101**, 1–17.
- FLASAR, F. M., R. E. SAMUELSON, AND B. J. CONRATH 1981. Titan's atmosphere: Temperature and dynamics. *Nature* **292**, 693–698.
- FLASAR, F. M., AND B. J. CONRATH 1992. The meteorology of Titan. In *Proceedings, Symposium on Titan*, pp. 89–95, ESA SP-338. Noordwijk, The Netherlands.
- FLASAR, F. M., M. D. ALLISON, AND J. I. LUNINE 1996. Titan zonal wind model. In *Huygens: Science, Payload and Mission*. ESA SP-1177. Noordwijk, The Netherlands, in press.
- GIERASCH, P. J. 1975. Meridional circulation and the maintenance of the Venus atmospheric rotation. *J. Atmos. Sci.* **32**, 1038–1044.
- HOUDIN, F., AND O. TALAGRAND 1996. Superrotation of planetary atmospheres: A numerical study. *J. Atmos. Sci.* submitted.
- HOUDIN, F., O. TALAGRAND, R. SADOURNY, R. COURTIN, D. GAUTIER AND C. P. MCKAY 1995. Numerical simulation of the general circulation of the atmosphere of Titan. *Icarus* **117**, 358–374.
- INGERSOLL, A. P. 1990. Dynamics of Triton's atmosphere. *Nature* **344**, 315–317.
- INGERSOLL, A. P., AND K. A. TRYKA 1990. Triton's plumes: The dust devil hypothesis. *Science* **250**, 435–437.
- LELLOUCH, E. 1994. The thermal structure of Pluto's atmosphere: Clear vs. hazy models. *Icarus* **108**, 255–264.
- LORENZ, E. N. 1967. *The Nature and Theory of the General Circulation of the Atmosphere*. WMO.
- MAROTZKE, J., AND J. WILLEBRAND 1991. Multiple equilibria of the global thermohaline circulation. *J. Phys. Ocean.* **21**, 1372–1385.
- NEWMAN, M., G. SCHUBERT, A. J. KLIORE, AND I. R. PATEL 1984. Zonal winds in the middle atmosphere of Venus from Pioneer Venus radio occultation data. *J. Atmos. Sci.* **41**, 1901–1913.
- NEWMAN, M., AND C. LEOVY 1992. Maintenance of strong rotational winds in Venus' middle atmosphere by thermal tides. *Science* **257**, 647–650.
- ROSSOW, W. B., AND G. P. WILLIAMS 1979. Large-scale motion in the Venus stratosphere. *J. Atmos. Sci.* **36**, 377–389.
- ROSSOW, W. B., A. D. DEL GENIO, AND T. P. EICHLER 1990. Cloud-tracked winds from Pioneer Venus OCPP images. *J. Atmos. Sci.* **47**, 2053–2084.
- SCHUBERT, G., C. COVEY, A. DEL GENIO, L. S. ELSON, G. KEATING, A. SEIFF, R. E. YOUNG, J. APT, C. C. COUNSELMAN, A. J. KLIORE, S. S. LIMAYE, H. E. REVERCOMB, L. A. SROMOVSKY, V. E. SUOMI, F. TAYLOR, R. WOO, AND U. VON ZAHN 1980. Structure and circulation of the Venus atmosphere. *J. Geophys. Res.* **85**, 8007–8025.
- SICARDY, B., A. BRAHIC, C. FERRARI, D. GAUTIER, J. LECACHEUX, E. LELLOUCH, F. ROQUES, J. E. ARLOT, F. COLAS, W. THUILLLOT, F. SEVRE, J. L. VIDAL, C. BLANCO, S. CRISTALDI, C. BUIL, A. KLOTZ, AND E. THOUVENOT 1990. Probing Titan's atmosphere by stellar occultation. *Nature* **343**, 350–353.
- STERN, S. A., AND L. TRAFTON 1984. Constraints on bulk composition, seasonal variation, and global dynamics of Pluto's atmosphere. *Icarus* **57**, 231–240.
- SUAREZ, M. J., AND D. G. DUFFY 1992. Terrestrial superrotation: A bifurcation of the general circulation. *J. Atmos. Sci.* **49**, 1541–1554.
- TYLER, G. L., D. N. SWEETNAM, J. D. ANDERSON, S. E. BORUTZKI, J. K. CAMPBELL, V. R. ESHELMAN, D. L. GRESH, E. M. GURROLA, D. P. HINSON, N. KAWASHIMA, E. R. KURINSKI, G. S. LEVY, G. F. LINDAL, J. R. LYONS, E. A. MAROUF, P. A. ROSEN, R. A. SIMPSON, AND G. E. WOOD 1989. Voyager radio science observations of Neptune and Triton. *Science* **246**, 1466–1473.
- YELLE, R. V., J. I. LUNINE, AND D. M. HUNTEN 1991. Energy balance and plume dynamics in Triton's lower atmosphere. *Icarus* **89**, 347–358.